Superconductivity close to the charge-density-wave instability

To cite this article: H. Bakrim and C. Bourbonnais 2010 *EPL* **90** 27001

A Letters Journal Exploring the Frontiers of Physics

April 2010

EPL, **90** (2010) 27001
doi: 10.1209/0295-5075/90/27001

www.epljournal.org

Superconductivity close to the charge-density-wave instability

H. Bakrim[1] and C. Bourbonnais[1,2(a)]

[1] *Regroupement Québécois sur le Matériaux de Pointe, Département de Physique, Université de Sherbrooke Sherbrooke, Québec, Canada, J1K-2R1*
[2] *Canadian Insitute for Advanced Research - Toronto, Ontario, Canada*

received 16 January 2010; accepted in final form 6 April 2010
published online 6 May 2010

PACS 74.20.Mn – Nonconventional mechanisms
PACS 71.45.Lr – Charge-density-wave systems
PACS 74.70.Kn – Organic superconductors

Abstract – We use the weak-coupling renormalization group method to examine the interplay between charge-density-wave and s-wave superconducting orders in a quasi–one-dimensional model of electrons interacting with acoustic phonons. The relative stability of both types of order is mapped out at arbitrary nesting deviations and Debye phonon frequency ω_D. We single out a power law increase of the superconducting $T_c \sim \omega_D^{0.7}$ from a quantum critical point of charge-density-wave order triggered by nesting alterations. The results capture the key features shown by the proximity between the two types of ordering in the phase diagram of the recently discovered Perylene-based organic superconductor under pressure. The impact of Coulomb interaction on the relative stability of the competing phases is examined and discussed in connection with the occurrence of s-wave superconductivity in low-dimensional charge-density-wave materials.

Introduction. – The recent observation of superconductivity (SC) in the Perylene-based organic conductor $Per_2[Au(mnt)_2]$ [1], brings once again into focus the possible role played by a charge-density-wave (CDW) instability in the mechanism of onset of SC in quasi–one-dimensional (quasi-1D) electron systems. This work makes use of the renormalization group (RG) technique to analyze the interplay between these two phases in systems of electrons coupled to lattice vibrations. Besides their relevance for materials showing a CDW-SC proximity, the results also address the issue of quantum criticality associated with interfering orders in models of electrons coupled to bosonic excitations in low dimensions [2,3].

$Per_2[Au(mnt)_2]$ is a member of the two-chain charge transfer salts series $Per_2[M(mnt)_2]$, where M = Pt, Pd, Au, ... These organic salts are made of Perylene and Dithiolate flat molecular complexes that pile up as segregated stacks well described by a quasi-1D electronic structure [4]. In normal pressure conditions, the Perylene chains undergo a metal-insulator transition due to the formation of a Peierls lattice-distorted state driven by a CDW superstructure [5]. For the $Per_2[Au(mnt)_2]$ compound, only the Perylene stacks are electronically active in the CDW transition, which takes place at $T_{\rm CDW} \simeq 12\,{\rm K}$ at ambient pressure [6]. This is a relatively low-temperature scale likely to be vulnerable to nesting alterations of the Fermi surface by the application of pressure. This is supported by the suppression of the insulating state under 5 kbar of pressure, which turns out to be also critical to the onset of SC at $T_c \simeq 300\,{\rm mK}$ [1], hinting at a direct part played by CDW correlations in the enhancement of Cooper pairing. The sequence of states thus obtained is reminiscent of the competition between CDW and SC orders found in some quasi-1D transition-metal trichalcogenides materials [7]. The pattern is also akin to the quasi-1D Bechgaard salts series $[(TMTSF)_2X]$, where a spin-density-wave (SDW) state is known to be followed by superconductivity under pressure [8–10]. In the latter case the application of the RG method to electron models with momentum-dependent repulsive interactions has demonstrated how nesting deviations can control the interference between density-wave and non–s-wave Cooper pairings and reproduce the sequence of phases displayed by the Bechgaard salts under pressure [11–13].

However, at variance with SDW systems where the direct Coulomb term dominates the scene of interactions, the electron-phonon coupling plays an essential role in lattice-distorted CDW systems. Electron-electron interactions induced by the exchange of acoustic phonons are

(a) E-mail: cbourbon@physique.usherbrooke.ca

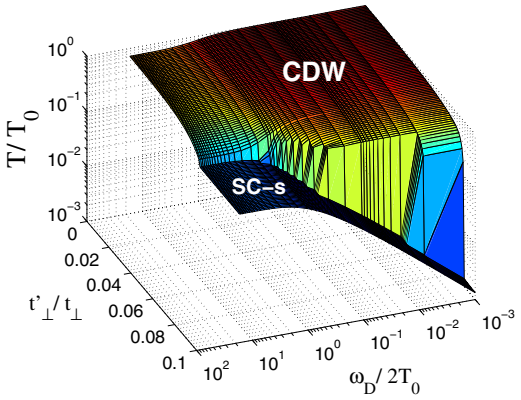

Fig. 1: (Colour on-line) Phase diagram of the quasi-1D electron-phonon model in the $(t'_\perp, \omega_D)$-plane. Here T_0 is the CDW ordering temperature of the adiabatic $\omega_D \to 0$ and perfect nesting $t'_\perp \to 0$ limit.

dynamically governed by the Debye energy scale ω_D, which is much smaller than the Fermi energy and often close to the energy scale of CDW order found in molecular conductors [8]. This introduces retardation in interactions, which besides interchain hopping and nesting alterations, modifies in a non-trivial way the interfering many-body processes that are linked to density-wave and Cooper pairings in every order of perturbation theory. This difficulty has been well established in the past, requiring to go beyond the habitual scheme of approximations such as mean-field and RPA-like approaches that are known to single out one pairing channel to the detriment of the other [14–16]. In the one-dimensional case, a weak-coupling solution to this problem has been found in the framework of the RG method [17,18]. Recent progress along these lines has shown that this approach is well suited to simultaneously account for both pairing processes in the determination of ground states in electron-phonon systems at arbitrary phonon frequency.

In this paper the RG method is extended to a electron-phonon model in the quasi-1D case and at finite temperature. The temperature scales $T_{\rm CDW}$ and T_c for the instabilities of the metallic state against the formation of CDW and SC orders are determined for arbitrary phonon frequency ω_D and nesting deviations parametrized by the next-to-nearest-neighbor interchain hopping $t'_\perp$. The main results of the present work are outlined in the phase diagram of fig. 1. For small $t'_\perp$, $T_{\rm CDW}$ weakens and undergoes a quantum-classical crossover as ω_D is raised and goes beyond the adiabatic scale T_0 for CDW ordering. When nesting distortion attains some threshold $t'^*_\perp$, $T_{\rm CDW}$ is critically reduced and at non-zero ω_D, an SC instability takes place in the s-wave channel only. In the adiabatic limit, $T_{\rm CDW}$ defines a quantum critical point at $t'^*_\perp$, from which an anomalous power law increase of T_c with the phonon frequency takes place. Along realistic pressure paths in the $(t'_\perp, \omega_D)$-plane, the model phase diagram follows the leading features displayed by $\mathrm{Per}_2[\mathrm{Au(mnt)}_2]$. The impact of the repulsive Coulomb interaction on the structure of the phase diagram is explored alongside the predisposition of electron-phonon driven CDW systems to show s-wave superconductivity.

The model and the renormalization group equations. – We consider a non–half-filled two-dimensional electron system consisting of $N_\perp$ chains of length L with the electron spectrum $E_p(\boldsymbol{k}) = v_F(pk - k_F) + \varepsilon_\perp(k_\perp)$, where $\varepsilon_\perp(k_\perp) = -2t_\perp \cos k_\perp - 2t'_\perp \cos 2k_\perp$. Here $p = \pm$ refers to right- and left-moving electrons along the stacks, $v_F(k_F)$ to the parallel Fermi velocity (wave vector), and $t_\perp$ to the interchain hopping integral. In the quasi-1D case, we have $t_\perp \ll E_F = v_F k_F$, where $E_F = E_0/2$ is the Fermi energy taken as half the band width. The next-to-nearest-neighbor transverse hopping $t'_\perp$, which describes nesting deviations, is kept small compared to $t_\perp$. The following calculations are carried out for the typical values $E_F = 15t_\perp = 3000\,\mathrm{K}$. In the framework of the Su-Schrieffer-Heeger (SSH) model [19], the electrons are linearly coupled to parallel acoustic phonons. These modes being harmonic, this is equivalent in the Matsubara formalism of the partition function to consider a frequency-dependent electron-electron interaction. In the g-ology picture, the bare interaction reads

$$g_i(\bar{k}_1, \bar{k}_2; \bar{k}_3, \bar{k}_4) = \frac{g_i^{\rm ph}}{1 + (\omega_{n_1} - \omega_{n_4})^2/\omega_D^2}, \qquad (1)$$

which for a non–half-filled band splits as a backward $(i = 1)$ and forward $(i = 2)$ scattering amplitude between $p = +$ and $-$ moving carriers; here the momentum-frequency variables $\bar{k} = (k_\perp, \omega_n)$ satisfy the conservation rule $\bar{k}_3 + \bar{k}_4 = \bar{k}_1 + \bar{k}_2$. For the SSH model the bare initial amplitude (normalized by πv_F) for the $2k_F$ backscattering part $g_1^{\rm ph}$ is non-zero ($g_1^{\rm ph} = -0.20$ in the following), while $g_2^{\rm ph} = 0$ for the forward scattering at vanishing momentum transfer [16].

To obtain the characteristic temperature scales for ordering in the presence of $t'_\perp$, the RG must be carried out at finite temperature. The RG transformation of the coupling constants results from the successive integration of electronic degrees of freedom in the outer energy shell $\pm E_0(\ell) d\ell/2$ above and below the Fermi surface for all Matsubara frequencies. Here $E_0(\ell) = E_0 e^{-\ell}$ is the scaled bandwidth at the step $\ell \geqslant 0$ varying from zero to infinity at finite T. In the momentum-frequency RG scheme adopted here at finite temperature, each constant energy sheet from the Fermi surface is divided into 12 patches, each defining a particular $k_\perp$ in momentum space, while a discrete set of $N_\omega = 14$ fermion Matsubara frequencies ω_n $(-7 \leqslant n \leqslant 6)$ is retained along the frequency axis. At finite temperature this represents a good compromise between exacting computing time and reproducing the results known for either the non-retarded case in quasi-one dimension [12] or the electron-phonon problem in one dimension [17].

At the one-loop level, the backward and forward scattering amplitudes obey the finite T flow equations

$$\partial_\ell g_1(\bar{k}_1,\bar{k}_2,\bar{k}_3,\bar{k}_4) = \frac{1}{2\pi}\int \mathrm{d}k_\perp I_P(k_\perp,\bar{q}_P) \times \big[\epsilon_P\langle g_1(\bar{k}_1,\bar{k},\bar{k}_P,\bar{k}_4)g_1(\bar{k}_P,\bar{k}_2,\bar{k}_3,\bar{k})\rangle + \epsilon_{P,v}\langle g_2(\bar{k}_1,\bar{k},\bar{k}_4,\bar{k}_P)g_1(\bar{k}_P,\bar{k}_2,\bar{k}_3,\bar{k})\rangle + \epsilon_{P,v}\langle g_1(\bar{k}_1,\bar{k},\bar{k}_P,\bar{k}_4)g_2(\bar{k}_P,\bar{k}_2,\bar{k},\bar{k}_3)\rangle\big] + \frac{1}{2\pi}\int \mathrm{d}k_\perp I_C(k_\perp,\bar{q}_C) \times \big[\epsilon_C\langle g_1(\bar{k}_1,\bar{k}_2,\bar{k},\bar{k}_C)g_2(\bar{k},\bar{k}_C,\bar{k}_4,\bar{k}_3)\rangle + \epsilon_C\langle g_2(\bar{k}_1,\bar{k}_2,\bar{k}_C,\bar{k})g_1(\bar{k},\bar{k}_C,\bar{k}_3,\bar{k}_4)\rangle\big] \quad (2)$$

and

$$\partial_\ell g_2(\bar{k}_1,\bar{k}_2,\bar{k}_3,\bar{k}_4) = \frac{1}{2\pi}\int \mathrm{d}k_\perp I_P(k_\perp,\bar{q}'_P) \times\epsilon_{P,l}\langle g_2(\bar{k}_1,\bar{k},\bar{k}_3,\bar{k}'_P)g_2(\bar{k}'_P,\bar{k}_2,\bar{k},\bar{k}_4)\rangle + \frac{1}{2\pi}\int \mathrm{d}k_\perp I_C(k_\perp,\bar{q}_C) \times \big[\epsilon_C\langle g_1(\bar{k}_1,\bar{k}_2,\bar{k},\bar{k}_C)g_1(\bar{k},\bar{k}_C,\bar{k}_4,\bar{k}_3)\rangle + \epsilon_C\langle g_2(\bar{k}_1,\bar{k}_2,\bar{k}_C,\bar{k})g_2(\bar{k},\bar{k}_C,\bar{k}_3,\bar{k}_4)\rangle\big]\,. \quad (3)$$

These consist of closed loop ($\epsilon_P=-2$), vertex corrections ($\epsilon_{P,v}=1$) and ladder ($\epsilon_{P,l}=1$) diagrams of the $2k_F$ electron-hole (Peierls) pairing, which combine with the ladder diagrams ($\epsilon_C=-1$) of the electron-electron (Cooper) pairing. Here $\bar{k}_P=\bar{k}+\bar{q}_P$, $\bar{k}'_P=\bar{k}+\bar{q}'_P$ and $\bar{k}_C=-\bar{k}+\bar{q}_C$, where $\bar{q}_{P,C}=(q_{\perp P,C},\omega_{P,C})$ corresponds to the Peierls $\bar{q}_P=\bar{k}_1-\bar{k}_4$, $\bar{q}'_P=\bar{k}_1-\bar{k}_3$ and Cooper $\bar{q}_C=\bar{k}_2+\bar{k}_1$ variables. To significantly improve convergence of each diagram at arbitrary finite temperature, the frequency convolution $\sum_{\omega_n} g_i g_j \mathcal{L}_{C,P}$ has been decoupled as $\langle g_i g_j\rangle\sum_{\omega_n}\mathcal{L}_{C,P}$. In this simplified scheme, $\langle\cdots\rangle = {N_\omega}^{-1}\sum_n\cdots$, stands as an average of the regular variation of couplings over the internal loop frequency variable, whereas the ℓ derivative of the Cooper and Peierls loops $I_{P,C}=\sum_{n=-\infty}^{+\infty}\mathcal{L}_{P,C}$ is evaluated exactly to give

$$I_{P,C}\ \ (k_\perp,\bar{q}_{P,C}) = \sum_{\nu=\pm1}\Theta[|E_0(\ell)/2+\nu A_{P,C}|-E_0(\ell)/2] \times\frac{1}{4}\left[\tanh\frac{E_0(\ell)+2\nu A_{P,C}}{4T}+\tanh\frac{E_0(\ell)}{4T}\right] \times\frac{(E_0(\ell)+\nu A_{P,C})E_0(\ell)}{(E_0(\ell)+\nu A_{P,C})^2+\omega_{P,C}^2}, \quad (4)$$

where $A_P=-\varepsilon(k_\perp)-\varepsilon(k_\perp+q_{\perp P})$, $A_C=-\varepsilon(k_\perp)+\varepsilon(k_\perp+q_{\perp C})$, and $\Theta(x)$ is the step function ($\Theta(0)\equiv\frac{1}{2}$) [12].

The RG equations are integrated from $\ell=0$ to $\ell\to\infty$ and a singularity can occur in either the Peierls or the Cooper scattering channel, which is indicative of an instability of the metallic state towards long-range order at the temperature T_μ. The nature of the ordering state is provided by the singularity of the static and normalized response function $\pi v_F\chi_\mu(\mathbf{q}^0_\mu)=(2\pi)^{-1}\iint \mathrm{d}k_\perp\mathrm{d}\ell$ $\langle z^2_\mu(\bar{k})\rangle I_{P,C}(k_\perp,q^0_{\perp,\mu})$ at the wave vector $\mathbf{q}^0_{\mathrm{CDW}}=(2k_F,\pi)$ for $\mu=\mathrm{CDW}$ and $\mathbf{q}^0_{\mathrm{SC}}=0$ for $\mu=\mathrm{SC}$. The response vertex parts z_μ are governed by the equations

$$\partial_\ell z_{\mathrm{CDW}}(\bar{k}+\bar{q}^0_P) = \frac{1}{2\pi}\int \mathrm{d}k'_\perp I_P(k'_\perp,\bar{q}^0_P) z_{\mathrm{CDW}}(\bar{k}'+\bar{q}^0_P) \times\big\langle[\epsilon_P g_1(\bar{k}'+\bar{q}^0_P,\bar{k},\bar{k}+\bar{q}^0_P,\bar{k}') + \epsilon_{P,v} g_2(\bar{k}'+\bar{q}^0_P,\bar{k},\bar{k}',\bar{k}+\bar{q}^0_P)]\big\rangle\,, \quad (5)$$

for the $\mu=$CDW response ($\bar{q}^0_P=(\pi,0)$) and

$$\partial_\ell z_{\mathrm{SC}}(-\bar{k}+\bar{q}^0_C) = \frac{1}{2\pi}\int \mathrm{d}k'_\perp I_C(k'_\perp,\bar{q}^0_C) z_{\mathrm{SC}}(-\bar{k}'+\bar{q}^0_C) \times\big\langle\epsilon_C[g_1(-\bar{k}'+\bar{q}^0_C,\bar{k}',-\bar{k}+\bar{q}^0_C,\bar{k}) + g_2(-\bar{k}'+\bar{q}^0_C,\bar{k}',\bar{k},-\bar{k}+\bar{q}^0_C)]\big\rangle, \quad (6)$$

for the static (s-wave) $\mu=$SC response ($\bar{q}^0_C=0$). For the whole range of parameters covered by the present model, the finite temperature singularities only occur for either the CDW or s-wave SC susceptibilities (fig. 2).

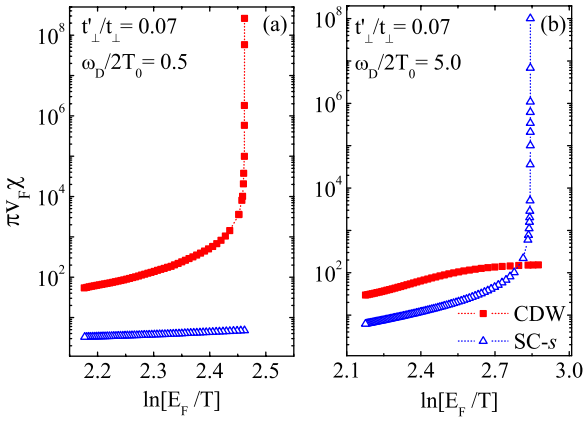

Fig. 2: (Colour on-line) Typical low-temperature dependence of the charge-density-wave (χ_{CDW}: squares) and s-wave superconducting (χ_{SC}: triangles) normalized susceptibilities in the a) CDW and b) SC ordering sectors of fig. 4.

Results. – Let us first consider the instability of the metallic state as one moves along the phonon frequency axis at fixed $t'_\perp$ (fig. 1). At perfect nesting $t'_\perp=0$, the adiabatic limit $\omega_D\to0$ is characterized by a singularity signaling the occurrence of a Peierls instability at the temperature denoted T_0 ($\simeq 20\,\mathrm{K}$ for the parameters chosen here). In this limit, only close loops contribute to the flow of eqs. (2), (3) and (5), a limit equivalent to the molecular field analysis of the Peierls instability of the metallic state. By increasing ω_D, both the vertex and ladder diagrams are progressively unlocked and begin to mix and interfere with closed loops. In the pertinent temperature range $T\ll t_\perp$ where all the instabilities take place, the transverse electronic motion is coherent. As a function of energy, the interference is then maximum in the one-dimensional part of the flow where $E_0(\ell)/2>t_\perp$, whereas for $E_0(\ell)/2<t_\perp$ interchain hopping begins to be coherent

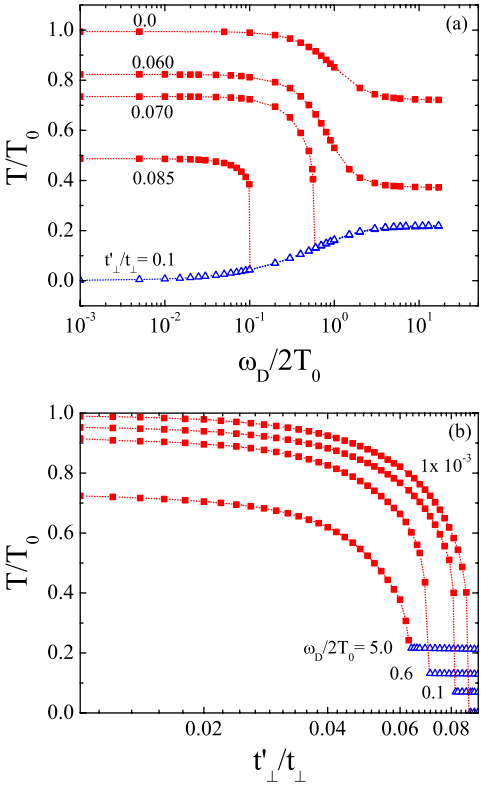

Fig. 3: (Colour on-line) (a) Normalized $T_{\rm CDW}$ (square) and s-wave T_c (triangle) *vs.* the phonon frequency ratio $\omega_D/2T_0$ at different $t'_\perp/t_\perp$. (b) Normalized $T_{\rm CDW}$ (square) and s-wave T_c (triangle) *vs.* the nesting deviation parameter $t'_\perp/t_\perp$ for different frequency ratios $\omega_D/2T_0$.

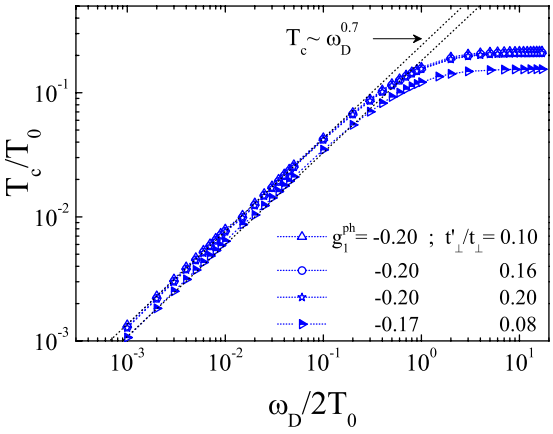

Fig. 4: (Colour on-line) Phonon frequency dependence of the superconducting ordering temperature T_c at different $t'_\perp < t'^*_\perp$ and electron-phonon coupling $g_1^{\rm ph}$. The dashed lines correspond to the power law $T_c \sim \omega_D^{0.7}$.

and the interference becomes non-uniform in momentum space and generates a $k_\perp$-dependence of the coupling constants [11,12]. As a result, $T_{\rm CDW}$ diminishes with increasing ω_D. However, when the frequency reaches the classical Peierls scale $\omega^*_D(t'_\perp = 0) \sim 2T_0$, the decrease is more rapid and $T_{\rm CDW}$ undergoes a crossover toward a non-adiabatic CDW regime where all diagrams of both pairing channels contribute and ultimately level off the reduction of $T_{\rm CDW}$ (fig. 3(a)) —a crossover analogous to the one found in the purely 1D case at $t_\perp = 0$ [16,17].

A finite amplitude of the antinesting term $t'_\perp$ modifies A_P in (4), which reduces all the Peierls diagrams but leaves those of the Cooper channel unchanged. Thus $T_{\rm CDW}$ first gets smaller (fig. 3(a)), then drops rapidly as the phonon frequency extends across ω^*_D, which is also smaller, to finally attain the non-adiabatic limit (fig. 3(a)). This reduction carries on until $t'_\perp$ reaches in its turn a critical value where ω^*_D signals a crossover toward a different instability of the metallic state where the Cooper pairing processes are prevailing and the instability is against s-wave SC at T_c. According to fig. 3(a), the SC critical temperature increases with ω_D and finally reaches a plateau above $\omega_D \sim 2T_0$, a scale apparently still tied to the adiabatic CDW limit. The s-wave Cooper pairing attraction is taking place along the chains and is strongly enhanced by CDW fluctuations (fig. 1(b)). The T_c values thus achieved are markedly enhanced with respect to the BCS limit obtained when all the Peierls loops in (2), (3) are put to zero.

When in the adiabatic limit, $t'_\perp$ is further increased up the critical value $t'^*_\perp \approx 0.9T_0$, nesting alterations are sufficiently large to suppress the singularity of the Peierls channel, bringing $T_{\rm CDW}$ down to zero (top curve, fig. 3(b)). Since at $\omega_D \to 0$, all the ladder diagrams are vanishingly small, the point $t'^*_\perp$ defines a quantum critical point for CDW ordering. Moving now away from this point, along the frequency axis, the SC instability shows up as a result of the ladder diagrams of the Cooper channel that progressively unfold. However, at variance with the single channel BCS approximation, T_c follows a power law increase $T_c \sim \omega_D^\eta$, with an exponent $\eta \simeq 0.70$ smaller than unity (fig. 4) —the BCS value $\eta \simeq 1$ being recovered when all the Peierls loops are turned off.

Being independent of $t'_\perp > t'^*_\perp$ and for a sizable range $g_1^{\rm ph}$ in weak coupling, the exponent η shows no noticeable trace of non-universality (fig. 4). The non-BCS increase of T_c is a direct consequence of the influence of CDW correlations on Cooper pairing and which takes place at all energy scales. As a matter of fact, when ω_D increases, the Cooper diagrams grow in importance on the one hand, but CDW correlations and then the pairing interaction is reduced on the other. It is the combination of both effects that leads to an exponent η smaller than unity. This contrasts with the BCS case where only the former effect is present, while the coupling is considered essentially fixed and attractive only below the sharp cutoff $E_0(\ell)/2 = \omega_D$ [20].

The "critical line" $T_c \sim \omega_D^\eta$ corresponds to a quantum-classical transition between the metallic and the SC states. The Debye frequency can thus be put in the category of a symmetry-breaking parameter that drives the transition at a fixed electron-phonon coupling. In the standard terminology [21], η is the crossover exponent $\phi = z\nu$ of

the transition expressed in terms of the product of the dynamical and coherence length exponents. Assuming Lorentz invariance of the model, this forces $z=1$, which would imply an anomalous dimension for the coherence length exponent, namely $\nu=\eta$. Interestingly, if one looks at the range of phonon frequency over which the power law for T_c takes place, one realized that it is confined to low frequency. According to figs. 3(a) and 4, T_c indeed levels off when ω_D exceeds the Peierls scale $2T_0$ for non-adiabaticity, stressing once again the non-BCS character of the transition.

To complete the analysis of the transition profile as a function of nesting deviations, one observes from fig. 3(b) that at finite ω_D, the weakening of $T_{\rm CDW}$ by ladder diagrams and vertex corrections is correlated to a reduction of the threshold value $t_\perp'^*$ for the onset of superconductivity. The decrease of T_c with increasing $t'_\perp > t_\perp'^*$ is found in fig. 3(b) to be relatively slow for any finite ω_D. In effect, $t'_\perp$ is more effective as a low-energy scale to cut the CDW singularity than to reduce CDW correlations responsible of the major part of the attractive pairing (fig. 2(b)).

The above one-loop RG results for the present model are summed up in the global phase diagram of fig. 1 for arbitrary nesting deviations and phonon frequency.

Connection with experiments. – The above results can apply to low-dimensional CDW systems where the electron-phonon interaction is the prevalent mechanism for ordering. This is distinctly possible in CDW compounds like $\mathrm{Per_2[Au(mnt)_2]}$ for which the flat Perylene molecular unit is rather large in size and polarizable. The resulting Coulomb interaction is thus expected to be small as corroborated by the weak enhancement of the electron spin susceptibility and nuclear spin-lattice relaxation rate reported for this material [22,23]. The electron-phonon model considered above can then in a first approximation be applied to the CDW-SC sequence displayed by the compound under pressure. Taking into consideration the pronounced quasi-1D anisotropy of this material [4], the $T_{\rm CDW}(\simeq 12\,\mathrm{K}$ [1,6]) observed in normal pressure conditions can be considered not too far below the optimal scale T_0 calculated at perfect nesting. The ω_D of the $2k_F$ acoustic phonons of the quarter-filled Perylene stacks, though not known with accuracy, can be at least be taken as few dozens of degrees. This fairly places the compound with a frequency ratio $\omega_D/2T_0>1$, and according to fig. 1, with favorable conditions for superconductivity under pressure. As pressure scales up both band parameters and phonon frequency[1], the system is likely to move from the CDW region ($t'_\perp < t_\perp'^*, \omega_D/2T_0>1$) toward SC where ($t'_\perp \gtrsim t_\perp'^*, \omega_D/2T_0>1$) in the ($t'_\perp, \omega_D$)-plane of fig. 1, a path congruent with the results of Graf *et al.* [1].

[1]Strickly speaking pressure also reduces the initial backscattering amplitude of $|g_1^{\rm ph}|\propto\kappa^{-1}$, mainly through the hardening of the phonon spring constant κ, an effect not included here and which would lead to an additional but smooth reduction of both $T_{\rm CDW}$ and T_c under pressure.

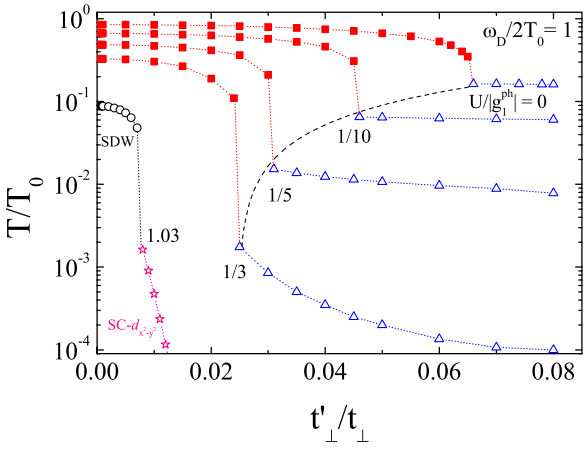

Fig. 5: (Colour on-line) Variation of the transition temperature ($T_{\rm CDW}$: squares; T_c: triangles) as a function of the antinesting parameter $t'_\perp$ for different Coulomb interaction amplitude $U/|g_1^{\rm ph}|$, normalized by $|g_1^{\rm ph}|$, along $U=2V$, and for $\omega_D/2T_0=1$. The dashed line gives the reduction of the maximum T_c with U. The circles (stars) refer to the SDW (d-wave SC) instability emerging for $U/|g_1^{\rm ph}|\gtrsim 1$.

The pairing attraction of the model, albeit boosted by CDW correlations, takes place along the chains and is responsible for the s-wave character of superconductivity. While a s-wave order parameter is well known to sustain the presence of non-magnetic impurities; on the contrary, it is sensitive to Coulomb interaction that is finite in practice and acts as a pair breaking effect. The impact the Coulomb term has on the above results can be readily examined by modifying the initial conditions of the flow equations (2) and (3). In the framework of the extended Hubbard model, this amounts to add the constant terms $g_1=U$ and $g_2=U+2V$ to the backward and forward scattering amplitudes at quarter-filling. Here $U>0$ and $V>0$ are the on-site and first nearest-neighbor repulsive *intra*-chain interaction parameters of the extended-Hubbard model, here normalized by πv_F.

From the foregoing analysis and for suitable conditions for superconductivity at $\omega_D/2T_0\sim 1$, the one-loop RG solution for the critical temperature along the line $U=2V$ is given in fig. 5 as a function of the antinesting parameter $t'_\perp$. While weak intra-chain Coulomb interaction reduces slightly $T_{\rm CDW}$ (essentially due to the repulsive backscattering component g_1), its detrimental impact on superconductivity is particularly pronounced for relatively weak repulsive interactions. The maximum T_c at $t_\perp'^*$ drops by an order of magnitude at $U\sim|g_1^{\rm ph}|/5$. However, it is worth noticing that such a range of U is sufficient to reduce the ratio $T_c/T_{\rm CDW}|_{\rm max}$ to values comparable with the one found experimentally in $\mathrm{Per_2[Au(mnt)_2]}$ [1] and in the inorganic trichalcogenide compound $NbSe_3$ [7].

By reinforcing repulsive interactions, T_c will therefore not be very long to become vanishingly small and potentially undetectable in practice, in spite of a sizable $T_{\rm CDW}$ at low pressure. This may supply some insight as to

why quarter-filled molecular compounds like TMTSF-DMTCNQ [24], known as a correlated CDW system [8,25], failed to show any sign of superconductivity following the suppression of its lattice-distorted state under pressure. Such an interpretation may also adhere to the absence of superconductivity in the phase diagram of correlated quasi-1D compounds like [EDT-TTF-CONMe$_2$]X [26], and (DI-DCNQI)$_2$X [27] at high pressure. From this angle, the chance for a correlated organic metal like TTF-TCNQ [8], whose CDW order is expected to vanish around 90 kbar [28], to show superconductivity is reduced at the very least in the s-wave channel.

We finally examine in fig. 5 the impact of further increasing the Coulomb term U on the phase diagram, namely beyond the amplitude of the phonon induced interaction. A qualitative change then occurs in the nature and the sequence of ground states. The CDW gives way to a SDW instability at low $t'_\perp$, which in its turn yields non-conventional d-wave superconductivity at $t'^*_\perp$ and above. It is where the results of the present work connect to the sequence of instabilities found in the purely repulsive case [11–13], which is known to apply in systems like the Bechgaard salts [8–10].

Conclusion. – In conclusion the instability of the metallic state against charge-density-wave and s-wave superconducting orders in quasi-1D systems can be analyzed by extending the RG approach to electrons coupled to phonons of arbitrary frequency. The results show that both instabilities influence one another and form a sequence of ordered states that captures the key traits of low-dimensional charge-density-wave materials exhibiting superconductivity under pressure.

* * *

CB thanks the National Science and Engineering Research Council of Canada (NSERC), the Réseau Québcois des Matériaux de Pointe (RQMP) and the *Quantum materials* program of Canadian Institute of Advanced Research (CIFAR) for financial support. Computational resources were provided by the Réseau Québécois de Calcul de Haute Performance (RQCHP) and Compute Canada.

REFERENCES

[1] Graf D. *et al.*, *EPL*, **85** (2009) 27009.
[2] Demler E., Sachdev S. and Zhang Y., *Phys. Rev. Lett.*, **87** (2001) 06702.
[3] Abanov A., Chubukov A. V. and Schmalian J., *Adv. Phys.*, **52** (2003) 119.
[4] Canadell E., Almeida M. and Brooks J., *Eur. Phys. J. B*, **42** (2004) 453.
[5] Henriques R. T., Alcacer L., Pouget J. P. and Jerome D., *J. Phys. C*, **17** (1984) 5197.
[6] Bonfait G. *et al.*, *Solid State Commun.*, **80** (1991) 391; Bonfait G., Matos M. J., Henriques R. T. and Almeida M., *Physica B*, **211** (1995) 297.
[7] Briggs A. *et al.*, *J. Phys. C*, **13** (1980) 2117.
[8] Jérome D. and Schulz H. J., *Adv. Phys.*, **31** (1982) 299.
[9] Vuletic T. *et al.*, *Eur. Phys. J. B*, **25** (2002) 319.
[10] Doiron-Leyraud N. *et al.*, *Phys. Rev. B*, **80** (2009) 214531.
[11] Duprat R. and Bourbonnais C., *Eur. Phys. J. B*, **21** (2001) 219.
[12] Nickel J. C., Duprat R., Bourbonnais C. and Dupuis N., *Phys. Rev. Lett.*, **95** (2005) 247001; *Phys. Rev. B*, **73** (2006) 165126.
[13] Bourbonnais C. and Sedeki A., *Phys. Rev. B*, **80** (2009) 085105.
[14] Barisic S., in *Electronic Properties of Inorganic Quasi-One-Dimensional Compounds, Ser. B, Quasi-one-dimensional Materials*, edited by Monceau P., (D. Reidel, Dordrecht) 1985, Part I, p. 1.
[15] Horovitz B., *Phys. Rev. B*, **16** (1977) 3943.
[16] Caron L. G. and Bourbonnais C., *Phys. Rev. B*, **29** (1984) 4230.
[17] Bakrim H. and Bourbonnais C., *Phys. Rev. B*, **76** (2007) 195115.
[18] Tam K.-M., Tsai S.-W., Campbell D. K. and Neto A. H. C., *Phys. Rev. B*, **75** (2007) 111103(R); in the 2D case, see Kilronomos F. D. and Tsai S.-W., *Phys. Rev. B*, **74** (2006) 205109; Honerkamp C., Fu H. C. and Lee D.-H., *Phys. Rev. B*, **75** (2007) 014503.
[19] Su W. P., Schrieffer J. R. and Heeger A. J., *Phys. Rev. B*, **22** (1980) 2099; see also Barisic S., *Phys. Rev. B*, **5** (1972) 932.
[20] In the BCS-Elisahberg theory, the ω_D-dependent reduction of the Coulomb pseudo-potential μ^* by the scattering in the electron-electron channel is well known to yield a power law isotope effect for $T_c \propto \omega_D^\alpha$, with α that differs from unity. See, for example, Morel P. and Anderson P. W., *Phys. Rev.*, **115** (1962) 1263; Carbotte J. P., *Rev. Mod. Phys.*, **62** (1990) 1027.
[21] Sachdev S., *Quantum Phase Transitions* (Cambridge University Press, Cambridge, UK) 1999.
[22] Almeida M. and Henriques R. T., in *Handbook of Organic Conductive Molecules and Polymers*, edited by Nalwa H. (Wyley, New York) 1997, p. 87.
[23] Bourbonnais C. *et al.*, *Phys. Rev. B*, **44** (1991) 641.
[24] Andrieux A. *et al.*, *J. Phys. (Paris)*, **40** (1979) 1199.
[25] Pouget J. P., *Chem. Scr.*, **55** (1981) 85.
[26] Auban-Senzier P. *et al.*, *Phys. Rev. Lett.*, **102** (2009) 257001.
[27] Itou T. *et al.*, *Phys. Rev. B*, **72** (2005) 113109.
[28] Yasuzuka S., Murata K., Arimoto T. and Kato R., *J. Phys. Soc. Jpn.*, **76** (2007) 033701.